ARTICLES
PUBLISHED ONLINE: 1 JUNE 2015 | DOI: 10.1038/NPHYS3339
nature physics

Measurement of the mobility edge for 3D Anderson localization

G. Semeghini[1], M. Landini[1,2], P. Castilho[1†], S. Roy[1], G. Spagnolli[1,2], A. Trenkwalder[1,2], M. Fattori[1,2], M. Inguscio[1,3] and G. Modugno[1,2*]

Anderson localization is a universal phenomenon affecting non-interacting quantum particles in a disordered environment. In three spatial dimensions, theory predicts a quantum phase transition from localization to diffusion at a critical energy, the mobility edge, which depends on the disorder strength. Although it has been recognized already long ago as a prominent feature of disordered systems, a complete experimental characterization of the mobility edge is still missing. Here we report the measurement of the mobility edge for ultracold atoms in a disordered potential created by laser speckles. We are able to control both the disorder strength and the energy of the system, so as to probe the position of the localization threshold in the disorder–energy plane. Our results might allow a direct experiment–theory comparison, which is a prerequisite to study the even more challenging problem of disorder and interactions.

In 1958, P. W. Anderson found that quantum particles in three-dimensional (3D) disorder are free to move only if their energy is above a critical energy E_c, whereas all energy states below E_c are localized[1]. The critical energy, which depends both on the disorder strength and on the disorder type, was later called the mobility edge[2], and it is now known to mark a true quantum phase transition[3]. Anderson localization and the Anderson transition have been the focus of intensive research for more than 50 years. Many aspects of the phenomenon are now well understood in the theory[4], but conclusive results about a fundamental quantity such as the mobility edge have not yet been achieved in experiments. The first context where the measurement was attempted was the electronic systems originally considered by the Anderson model. Although it is possible to study experimentally the metal–insulator transition[5], interactions between electrons are expected to change completely the localization problem[6–9]. Anderson localization has been studied also with other systems that are naturally non-interacting. For example, sound and light waves are being employed to measure the mobility edge essentially as a critical wavevector for localization[10,11]. Atomic kicked rotors, where localization happens in momentum space, allow one to study precisely the critical properties of the Anderson transition[12–15]. Ultracold atomic gases in disordered optical potentials are appealing because they allow one to simulate the physics of non-interacting electrons in a disordered environment with variable dimensionality[16–19]. They represent in principle a well-suited system to study the mobility edge in energy space and to determine its dependence on the disorder strength. Two recent experiments have indeed reported the observation of the Anderson transition in three dimensions[18,19]. However, a precise measurement of the mobility edge has been prevented so far by an incomplete control of the energy, because not only is it difficult to prepare a sample of atoms at a specific energy in the localized regime, but it is also difficult to measure their energy distribution in the disorder.

In this work we develop new techniques to prepare ultracold atomic samples in a disordered potential with a narrow energy distribution, and also to control and measure this distribution. These allow us not only to perform a measurement of E_c for a given disorder strength, but also to measure the trajectory of E_c in the disorder–energy plane.

Our energy-control strategy is based on three key parts. First, we employ a finite atomic interaction to load a Bose–Einstein condensate into the low-energy states of a disordered potential. By studying the transport properties of the cloud, we observe a crossover to full localization when increasing the disorder strength. We reconstruct the total energy distribution of the localized samples by combining measurements of their kinetic energy with numerical simulations of the low-energy states. Finally, we exploit the capability of varying the disorder strength in time to produce excitations with controlled energy, and we deduce E_c from a measurement of the energy needed to restore diffusion.

Preparation of localized samples

The ultracold samples consist of about 10^5 ^{39}K atoms, whose interactions can be controlled using a magnetic Feshbach resonance[20]. The disorder is generated by two coherent speckle fields[19] that are blue-detuned from the atomic transitions, producing a repulsive potential. Figure 1 shows the geometry and the calculated properties of the speckle potential, which are based on parameters directly measured in the experiment (see Supplementary Sections 1 and 2 for details). The two speckles cross each other at 90° with parallel linear polarizations, creating a 3D intensity distribution with anisotropic correlations. The two relevant energy scales are the disorder strength V_R, which represents both the mean value of the potential and its standard deviation[21], and the correlation energy $E_R = \hbar^2/m\sigma_R^2$, where $\hbar$ is the reduced Planck constant, m is the ^{39}K mass and σ_R is the mean correlation length of the disorder.

V_R can be controlled in the range $V_R/k_B = 0$–100 nK (where k_B is the Boltzmann constant) by changing the total speckle power; we carefully calibrated it with a 10% uncertainty, using two independent methods (see Supplementary Section 3 for details). The

[1]LENS and Dipartimento di Fisica e Astronomia, Universitá di Firenze, Via N. Carrara 1, 50019 Sesto Fiorentino, Italy. [2]CNR-INO, Via N. Carrara 1, 50019 Sesto Fiorentino, Italy. [3]INRIM, Strada delle Cacce 91, 10135 Torino, Italy. †Present address: Instituto de Física de São Carlos, Universidade de São Paulo, C.P. 369, 13560-970 São Carlos, SP, Brazil. *e-mail: modugno@lens.unifi.it

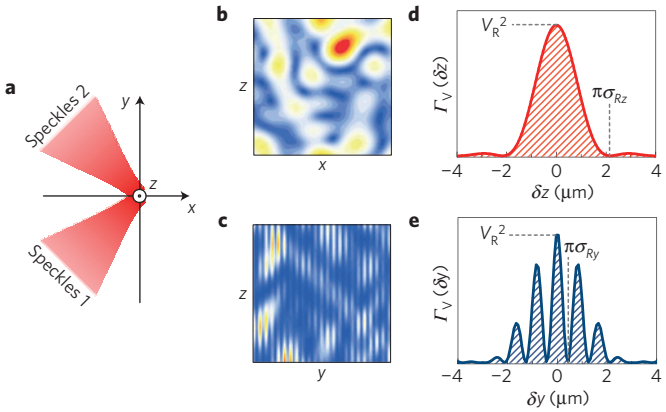

Figure 1 | 3D speckle disorder. a, Scheme of the speckle geometry. **b**,**c**, Example of the calculated disordered potential along two principal planes (each square has a size of 12.5 μm × 12.5 μm). **d**,**e**, Calculated potential autocorrelation functions. Along x and z, Γ_V follows the Bessel-type profile typical of speckle patterns[21] (shown here in **d** in the z direction as an example). The correlation length is calculated from the position of the first zero in Γ_V, so that $\pi\sigma_{Rx,z}$ are 3.39 μm and 2.38 μm respectively. Along y, an extra modulation coming from interference reduces the correlation length to $\pi\sigma_{Ry} = 0.28$ μm.

two speckle envelopes are Gaussian with waists of about 1,300 μm, much wider than the typical atomic distributions, ensuring the homogeneity of V_R. By defining the correlation lengths as in Fig. 1, we obtain $\pi\sigma_R = 1.30(6)$ μm from the geometric average in the three main directions. This leads to $E_R/k_B = 73(7)$ nK. For these characteristic energies, theory indicates that E_c should be comparable to V_R (refs 22–25).

The atomic sample is initially cooled down to Bose–Einstein condensation in a harmonic trap, in the presence of repulsive interactions[26]. Figure 2a shows a scheme of the loading procedure in the disordered potential, which consists of: a linear increase of V_R in 100 ms; a linear decrease of the trap strength to zero and a decrease of the interaction strength proportional to $1/t$ (where t is the time) down to a scattering length $|a| \leq 0.2\, a_0$ (a_0 is the Bohr radius), both lasting 200 ms. This procedure was optimized by minimizing the final kinetic energy. We then let the system evolve in the disordered potential for a variable time and we finally image the spatial distribution using absorption imaging along the z direction of Fig. 1. We study in particular the 1D density distribution $n(x)$, obtained from integration along two spatial dimensions (see Supplementary Section 4 for details). All measurements are averaged over different realizations of the disorder, obtained by rotating in steps one of the diffusive plates creating the speckles. We found that 5 realizations are typically enough to obtain stationary results, presumably because each sample contains a relatively large number of states, resulting in a self-averaging.

Measuring the second moment $\langle x^2\rangle = \int x^2 n(x)\mathrm{d}x$, we observe a strong dependence of the expansion dynamics on V_R, as shown in Fig. 2c. For small V_R, the evolution is purely diffusive, according to $\Delta\langle x^2\rangle(t) = \langle x^2(t)\rangle - \langle x^2(0)\rangle = 2Dt$, where D is the diffusion coefficient. Increasing V_R above $k_B \times 8$ nK, we observe a clear deviation from the diffusive behaviour. The decreasing rate of expansion with increasing time (data for $V_R/k_B = 23(2)$ nK, 47(5) nK and 94(9) nK in Fig. 2c) indicates the presence of a localized fraction that stops expanding after reaching its equilibrium size and does not contribute to any further increase of $\langle x^2\rangle$. For the largest V_R, the long-term behaviour is compatible with a plateau, suggesting a localized fraction close to unity. Looking at the time evolution of $n(x)$ in Fig. 2b, one can recognize a central part of the sample that is essentially stationary, while the tails expand in the first one second and then reach a steady configuration. This observation suggests the coexistence of different localization lengths, and therefore an energy distribution with finite width. From the tails of $n(x)$ at long times we measure a typical localization length of about 30 μm, whose order of magnitude is compatible with theoretical predictions[24] (see Supplementary Section 5 for details).

A quantitative study of the short-time dynamics confirms the onset of localization. We estimate the slope of the initial increase of $\langle x^2\rangle$ from a linear fit on the first 300 ms and we extract an initial diffusion coefficient D. The data, shown in Fig. 2d, indicate that the breakdown of the purely diffusive behaviour for $V_R/k_B > 8$ nK corresponds to an abrupt reduction below $D \approx \hbar/3m$. This is indeed the predicted regime where quantum interference suppresses diffusion and leads to localization[21,27].

Reconstruction of the energy distribution

The observation of a rather sharp onset of localization suggests that the energy spread of the system is narrow. Experimentally, we can access only the kinetic energy, or more precisely the momentum distribution, whereas the potential energy is impossible to measure directly. The momentum distribution is measured through a time-of-flight technique: after loading the sample into the speckles, we release it abruptly and we reconstruct the 1D momentum distribution $n(k)$ along the x direction from the time evolution of the density (see Supplementary Section 6 for details). We find that $n(k)$ is typically Gaussian, as shown in Fig. 3a. In the regime where we observe a localized fraction from the $\langle x^2\rangle$ measurements, we find that the mean kinetic energy lies well below V_R.

We then perform a numerical study of the low-energy eigenstates by exact diagonalization of the system's Hamiltonian to reconstruct the total energy distribution $n(E)$ from the measured $n(k)$. Numerical simulations are notoriously hard for energies close to the mobility edge, owing to the finite spatial size in the simulations, but we found that a box with side length of about $10\pi\sigma_R$ could give reliable results in the low-energy range occupied by the system (see Supplementary Section 7 for details). We calculate in particular the spectral function $\rho(E,k)$, which represents the probability for a state at energy E to have momentum k (ref. 28). It allows reconstruction of the energy distribution of the system from $n(k)$, through the standard relation $\int\rho(E,k)f(E)\mathrm{d}E = n(k)$, where $f(E)$ is the average occupation probability of the states at energy E. First, we search for the $f(E)$ that best reproduces the experimental $n(k)$. We find a very good agreement using an exponential form $f(E) \propto \exp(-E/E_m)$. The parameter E_m, which corresponds to an effective temperature of the system, is found by fitting the integral form to the experimental $n(k)$, as shown in Fig. 3a. The energy distribution is then determined as usual as $n(E) = \int\rho(E,k)\, f(E)\mathrm{d}k$ (note that $\int\rho(E,k)\mathrm{d}k$ is the density of states). Figure 3b shows the measured $n(E)$ for a relatively strong disorder, for which we observe a large localized fraction from the $\langle x^2\rangle$ measurement. One sees that $n(E)$ is narrow and peaked at an energy E_p not far from the lowest significant energy, which we label E_0 (the density of states is expected to have a weak Lifshits tail extended towards zero energy[29], which however cannot be detected with our numerical simulations). Assuming $E_c \approx V_R$, as predicted by theory, this energy distribution is consistent with a large localized fraction, as was suggested by the measurement of $\Delta\langle x^2\rangle(t)$.

Excitation procedure and determination of E_c

The final step to determine E_c consists of producing a controlled energy excitation in the system, so as to promote $n(E)$ towards diffusive states. After loading the atoms into the disordered potential, we apply a weak sinusoidal modulation to the speckle laser power for 0.5 s, corresponding to a time-dependent perturbation of the potential of the type $V_R(t) = V_R(1 + A\cos(\omega t))$, with $A \simeq 0.2$ and variable frequency ω. As we are in the small-A

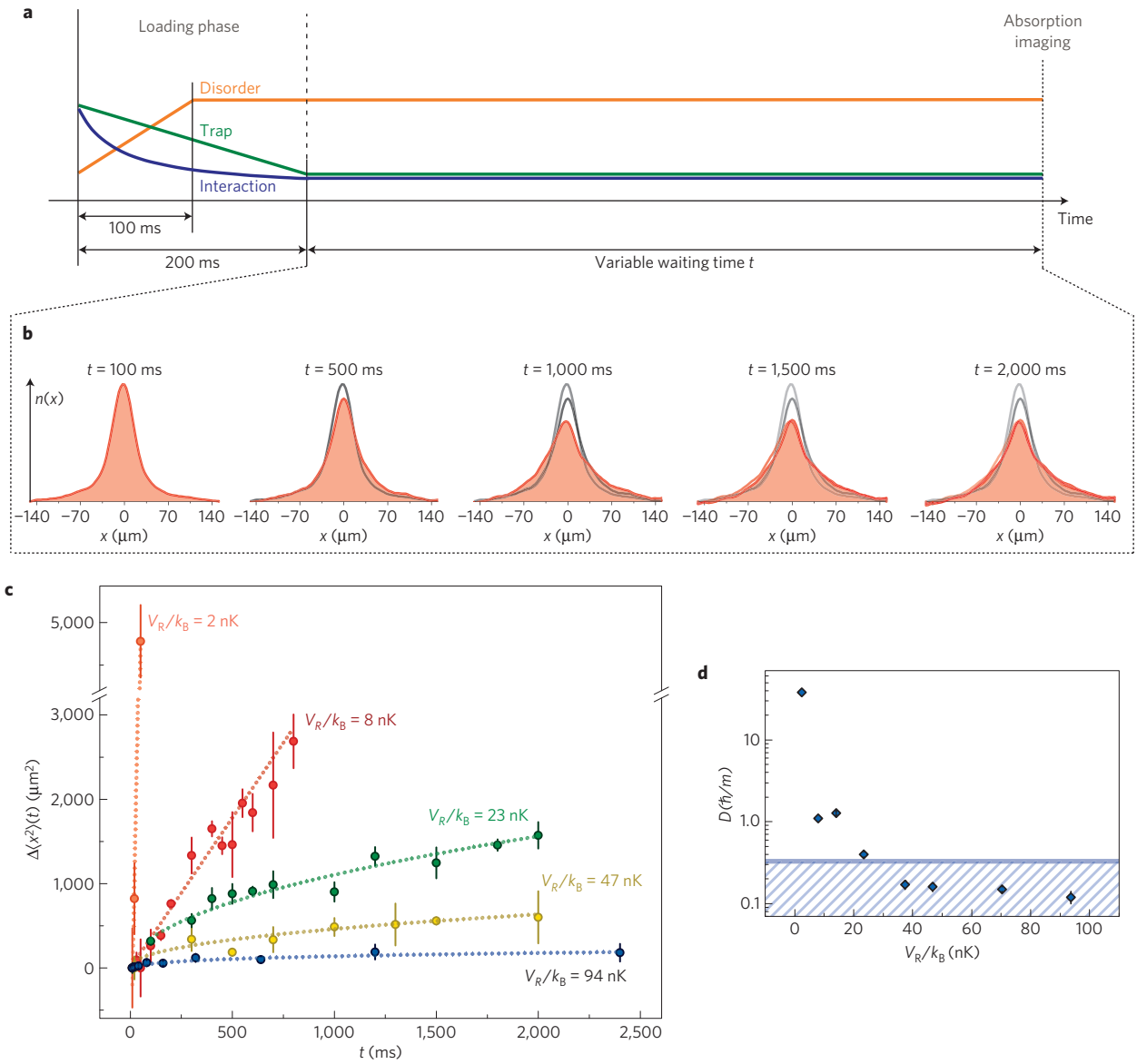

Figure 2 | Expansion and localization dynamics. a, Schematic diagram of the experimental procedure used to load the atoms in the disordered potential and to observe their diffusive or localized behaviour. **b**, Time evolution of the 1D density profile $n(x)$ for $V_R/k_B = 47(5)$ nK (grey lines on the background represent the profile at earlier times). **c**, Time evolution of $\Delta\langle x^2\rangle$ for different disorder strengths. The lines are a guide to the eye. **d**, Short-time diffusion coefficient. The shaded area is the regime of quantum transport, $D < \hbar/3m$, predicted by theory[21,27]. The error bars represent the statistical uncertainty and correspond to one standard deviation.

limit (see Supplementary Section 8 for details), this procedure allows excitation of a fraction of the system by exactly $\Delta E = \hbar\omega$. The energy distribution after the modulation can be written as $n'(E,\hbar\omega) = (1-p)n(E) + pn(E-\hbar\omega)$, where $p = p(E,\omega)$ is the probability to excite an atom from energy E to $E+\hbar\omega$. Despite p being in principle dependent on both E and ω, we estimate through numerical simulations that in the relevant range of energies this dependence is sufficiently weak to allow the assumption that p is constant (see Supplementary Section 8 for details). At the end of the modulation sequence we leave the disorder at fixed V_R for another 0.5 s, allowing the atoms transferred to diffusive states to expand enough to be effectively invisible to our imaging system. The transfer to diffusive states is hence detected as atom losses.

Figure 4c shows an example of the variation of the final atom number N as a function of the transferred energy $\hbar\omega$. To determine E_c we fit these data with $N_{loc}(E_c,\hbar\omega) = \int_0^{E_c} n'(E,\hbar\omega)\mathrm{d}E$, where the mobility edge E_c is the only free parameter. For simplicity, we do not use directly the discrete data for $n(E)$, but a fitted function of the form $n(E) = (E-E_0)^\alpha \exp(-(E-E_0)/E_m)$, as shown in Fig. 3b. For the specific data set in Fig. 4 we obtain $E_c/k_B = 50(6)$ nK. The agreement between the data and the model is in general very good until a large-ω regime where N increases again. This behaviour can be justified considering the reduced overlap in momentum space between deeply localized states and the essentially free states high in the continuum, which reduces the excitation probability p. In the absence of a precise model, we exclude the data at high frequency from the fit.

We note that our measurements of the number of localized atoms are performed on a spatial region of finite size and after a finite time. This may limit our ability to identify slowly diffusing atoms, potentially leading to a shift of the measured E_c. Our field of view is determined by experimental constraints, such as the finite signal-to-noise ratio, and cannot be changed, but we can change the observation time. Increasing the waiting time after the modulation

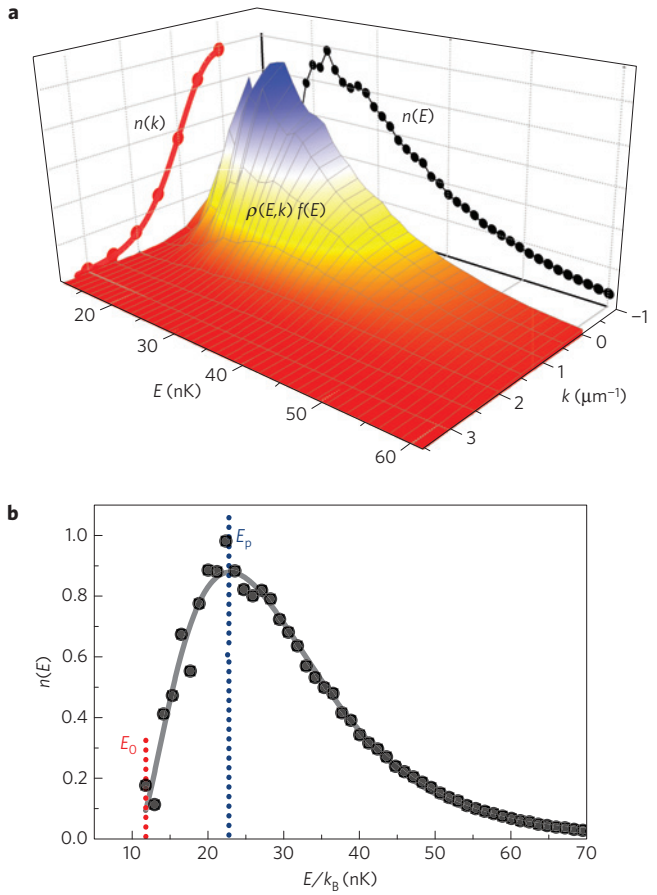

Figure 3 | Momentum and energy distribution. a, Schematic of the reconstruction process of $n(E)$ at $V_R/k_B = 47(5)$ nK: the occupation probability $f(E)$ is found so that the values of $\int \rho(E,k)\, f(E) dE$ (red dots) from the calculated $\rho(E,k)$ match with the experimental $n(k)$ (red line). The calculations are performed on a discrete grid with spacing of 0.5 μm^{-1} and 2 nK in momentum and energy, respectively. **b**, Expanded view of the reconstructed $n(E)$. The data (dots) are fitted with the model described in the text (line).

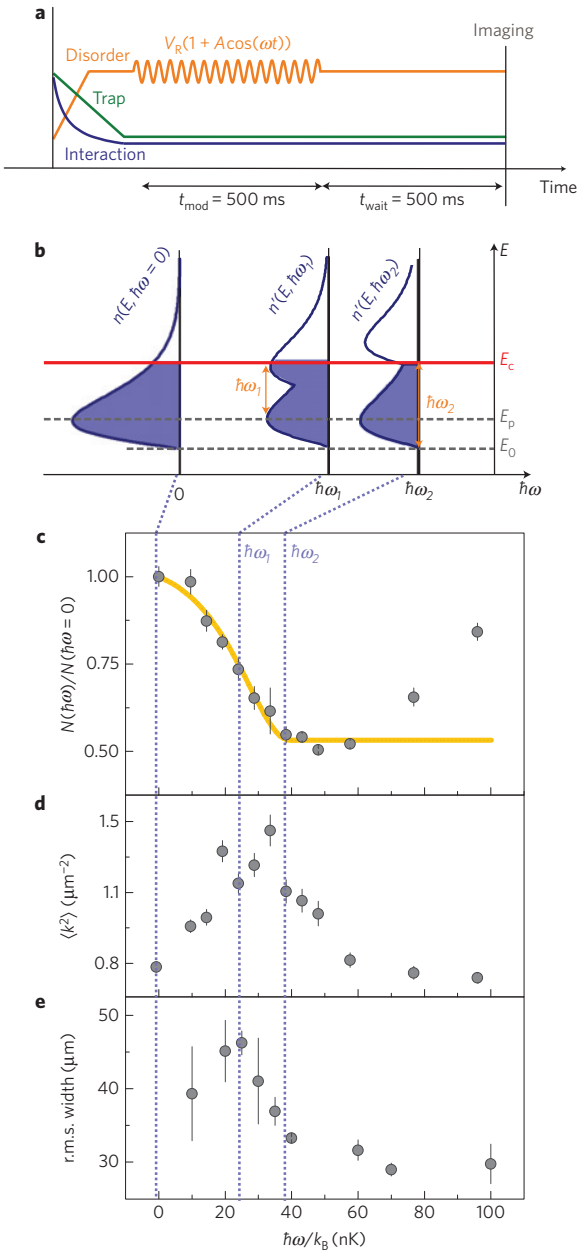

Figure 4 | Excitation spectrum. a, Schematic diagram of the experimental procedure used to produce controlled excitation on a localized sample. **b**, During the time modulation of the disordered potential, a fraction of the initial energy distribution gets shifted to higher energies by $\hbar\omega$, where ω is the modulation frequency. For sufficiently high ω, part of $n(E)$ is excited above E_c and then diffuses away during the following waiting time. **c**–**e**, At the end of t_{wait} we record the atom number (**c**), the kinetic energy (**d**) and the spatial size (**e**) of the cloud as a function of ω. The data reported here are for $V_R/k_B = 47(5)$ nK. The error bars represent the statistical uncertainty and correspond to one standard deviation. A fit of the atom number with the excitation model described in the text (yellow line) gives the mobility edge at $E_c/k_B = 50(6)$ nK. Placing this threshold on the energy distributions in **b** one can realize that the positions of the maximum size and kinetic energy (at $\hbar\omega_1$) and of the minimum atom number (at $\hbar\omega_2$) in the spectra are consistent with the features of the corresponding $n(E,\hbar\omega_{1,2})$ as explained in the text.

actually corresponds to an increased sensitivity of our measurement to the small D values close to the mobility edge. Repeating the same measurement as in Fig. 4a with a doubled waiting time (1 s) we actually observe a shift of E_c to lower energies by about 6 nK, comparable to the statistical uncertainty, which suggests the presence of a residual, slowly diffusive component. We treated this shift as a systematic error in the measurement of E_c at a waiting time of 0.5 s, adding it to the statistical uncertainty (see Supplementary Section 8 for more details).

It is worth noting that this estimation of E_c is mainly sensitive to the position of the plateau in $N(\omega)$, that is, to the modulation frequency ω_2 for which the whole excited fraction of $n'(E)$ is brought above E_c. It is straightforward to see that $\hbar\omega_2 = (E_c - E_0)$, as shown in Fig. 4b. This fact highlights the robustness of our determination of E_c, which essentially depends on two well-controlled quantities: the minimum energy E_0, which is reliably calculated numerically, and the frequency ω_2, which is experimentally determined. For example, from $\hbar\omega_2/k_B = 38(6)$ nK determined directly from the data in Fig. 4c and $E_0/k_B = 12$ nK from Fig. 3b, one would obtain $E_c/k_B = 50(6)$ nK as from the detailed modelling used in the fit of Fig. 4c.

An important test of the validity of our model is provided by additional measurements of the variation of both system size and kinetic energy with ω, shown in Fig. 4d,e. We observe that these two quantities reach a maximum value around the same excitation energy $\hbar\omega_1/k_B = 25(6)$ nK. This energy is apparently just below the energy $(E_c - E_p)$ that is necessary to excite the peak of the initial distribution to the mobility edge (see Fig. 4b) and should therefore

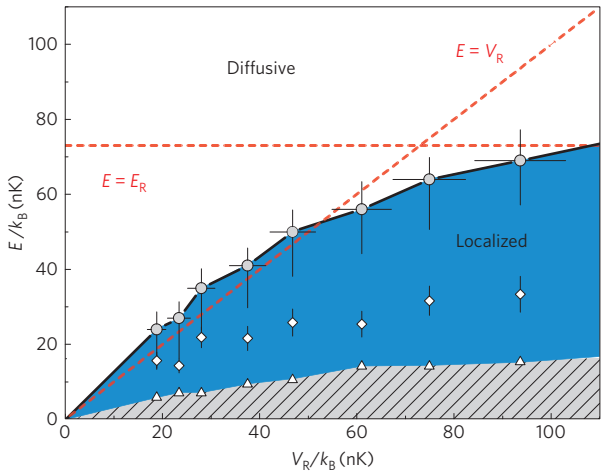

Figure 5 | Measured mobility edge versus the disorder strength. Trajectory of E_c (circles) separating localized from diffusive states. White diamonds are the peak energies E_p of $n(E)$ and white triangles are the lowest energies E_0. The errors bars for E_p represent the statistical uncertainty in the determination of $n(E)$. The vertical error bars for E_c contain the statistical uncertainties in the determination of $n(E)$ and in the fit of $N(\omega)$, and also the systematic uncertainty from the finite waiting time; the horizontal ones represent the uncertainty in the determination of V_R. All error bars correspond to one standard deviation.

correspond to an optimal transfer to localized states just below E_c, which have the largest localization lengths and the largest energies, as observed.

We repeated the excitation procedure for several disorder strengths. Figure 5 reports the measured trajectory for E_c in the disorder–energy plane. Most of our data are in the regime of $V_R < E_R$. This is considered as the most interesting regime for localization, because here the transport of particles is suppressed only owing to interference between quantum reflections by many potential barriers. In this regime the spatial correlations of the disorder should not have a dominant role, because E_c is smaller than the correlation energy E_R. We observe that up to $V_R/k_B = 47(5)$ nK our data are consistent with a linear scaling of E_c with V_R. When V_R is increased above E_R, the spatial correlations of the disorder start to play a role and atoms can also be trapped inside individual deep wells of the speckle potential. In this regime we observe instead a clear reduction of the slope of E_c.

Recent theoretical studies for similar types of speckle disorder[22–25,30] predict a qualitatively similar trajectory for E_c, with a regime at weak disorder in which E_c stays not far from V_R, and a strong-disorder regime in which E_c drops well below V_R. There is however a clear difference between our measurements and the theory, because the latter predicts that also at small disorder strengths E_c should stay below V_R, whereas our data are at or above V_R. For example, our results for $V_R < E_R$ are about 40% higher than those obtained for isotropic speckles with a transfer-matrix numerical method[25], an approach that is considered exact. The anisotropy of the speckle potential is however expected to have a non-negligible influence on the position of E_c (refs 23,24,30). In our case one should expect an increase of E_c with respect to the isotropic case, because the presence of interference along one direction tends to shift the system slightly towards a 2D system, where E_c is known to be infinite. A recent theoretical study that considers a geometry of crossed speckles as in our experiment confirms that E_c should increase towards V_R for moderate disorder strengths[31]. However, even considering the relatively large error bars in the experiment, there is still a disagreement between our results and the theory that will deserve a careful analysis[31].

We note that a larger mobility edge, $1.5V_R < E_c < 2V_R$, has been reported in a previous experimental study with ultracold atoms[18,32]. The short timescale used in the experiment and the neglected disorder potential energy in the analysis have raised concerns about the validity of this result[33,34]. A second experimental study[19] was instead performed on a long timescale and provided a precise measurement of the localized fraction of the system that is in agreement with a calculation of the mobility edge[23]. However, a direct determination of E_c has not been possible, in the absence of a direct measurement of $n(E)$.

Conclusion and outlook

In conclusion, we have experimentally determined the mobility edge trajectory in a system with controlled 3D disorder and tunable energy. Our technique is general for ultracold atoms and can be applied to other types of disorder, for example, to other types of correlation or to disordered lattices. A further narrowing of the energy distribution might also allow one to verify the critical exponents of the Anderson transition[3,14], for example by measuring the increase of the localization length for energies approaching the mobility edge. A full assessment of the non-interacting problem is also a prerequisite for exploring the challenging problem of disordered interacting systems, where even reliable theoretical predictions are difficult to obtain. For example, studying how the mobility edge is affected by a weak interaction would allow one to explore the open problem of many-body localization[9]. The control of disorder and interaction in three dimensions can also allow one to clarify fundamental aspects of Bose–Einstein condensation in disorder[35–37] for which only a limited number of experiments exist so far[38–40].

Received 6 January 2015; accepted 21 April 2015; published online 1 June 2015

References

1. Anderson, P. W. Absence of diffusion in certain random lattices. *Phys. Rev.* **109,** 1492–1505 (1958).
2. Mott, N. F. Metal–insulator transitions. *Phys. Today* **31**(11), 42–47 (1978).
3. Evers, F. & Mirlin, A. D. Anderson transitions. *Rev. Mod. Phys.* **80,** 1355–1417 (2008).
4. Abrahams, E. (ed.) *50 Years of Anderson Localization* (World Scientific, 2012).
5. Katsumoto, S., Komori, F., Sano, N. & Kobayashi, S. Fine tuning of metal-insulator transition in $Al_{0.3}Ga_{0.7}As$ using persistent photoconductivity. *J. Phys. Soc. Jpn* **56,** 2259–2262 (1987).
6. Lee, P. A. & Ramakrishnan, T. V. Disordered electronic systems. *Rev. Mod. Phys.* **57,** 287–337 (1985).
7. Vollhardt, D. & Wölfle, P. in *Electronic Phase Transitions* (eds Hanke, W. & Kopaev, Yu. V.) 1–78 (Elsevier, 1992).
8. Kramer, B. & MacKinnon, A. Localization: Theory and experiment. *Rep. Prog. Phys.* **56,** 1469–1564 (1993).
9. Basko, D. M., Aleiner, I. L. & Altshuler, B. L. Metal–insulator transition in a weakly interacting many-electron system with localized single-particle states. *Ann. Phys.* **321,** 1126–1205 (2006).
10. Hu, H. *et al.* Localization of ultrasound in a three-dimensional elastic network. *Nature Phys.* **4,** 845–848 (2008).
11. Sperling, T. *et al.* Direct determination of the transition to localization of light in three dimensions. *Nature Photon.* **7,** 48–52 (2013).
12. Chabé, J. *et al.* Experimental observation of the Anderson metal–insulator transition with atomic matter waves. *Phys. Rev. Lett.* **101,** 255702 (2008).
13. Lemarié, G., Lignier, H., Delande, D., Szriftgiser, P. & Garreau, J. C. Critical state of the Anderson transition: Between a metal and an insulator. *Phys. Rev. Lett.* **105,** 090601 (2010).
14. Lopez, M., Clément, J-F., Szriftgiser, P., Garreau, J. C. & Delande, D. Experimental test of universality of the Anderson transition. *Phys. Rev. Lett.* **108,** 095701 (2012).
15. Lopez, M. *et al.* Phase diagram of the anisotropic Anderson transition with the atomic kicked rotor: Theory and experiment. *New J. Phys.* **15,** 065013 (2013).
16. Billy, J. *et al.* Direct observation of Anderson localization of matter-waves in a controlled disorder. *Nature* **453,** 891–894 (2008).
17. Roati, G. *et al.* Anderson localization of a non-interacting Bose–Einstein condensate. *Nature* **453,** 895–898 (2008).

18. Kondov, S. S. *et al.* Three-dimensional Anderson localization of ultracold matter. *Science* **334,** 66–68 (2011).
19. Jendrzejewski, F. *et al.* Three-dimensional localization of ultracold atoms in an optical disordered potential. *Nature Phys.* **8,** 398–403 (2012).
20. Roati, G. *et al.* ^{39}K Bose–Einstein condensate with tunable interactions. *Phys. Rev. Lett.* **99,** 010403 (2007).
21. Shapiro, B. Cold atoms in the presence of disorder. *J. Phys. A* **45,** 143001 (2012).
22. Yedjour, A. & Van Tiggelen, B. A. Diffusion and localization of cold atoms in 3D optical speckle. *Eur. Phys. J. D* **59,** 249–255 (2010).
23. Piraud, M., Pezzé, L. & Sanchez-Palencia, L. Matter wave transport and Anderson localization in anisotropic three-dimensional disorder. *Eur. Phys. Lett.* **99,** 50003 (2012).
24. Piraud, M., Pezzé, L. & Sanchez-Palencia, L. Quantum transport of atomic matter waves in anisotropic two-dimensional and three-dimensional disorder. *New J. Phys.* **15,** 075007 (2013).
25. Delande, D. & Orso, G. Mobility edge for cold atoms in laser speckle potentials. *Phys. Rev. Lett.* **113,** 060601 (2014).
26. Landini, M. *et al.* Direct evaporative cooling of ^{39}K atoms to Bose–Einstein condensation. *Phys. Rev. A* **86,** 033421 (2012).
27. Kuhn, R. C., Sigwarth, O., Miniatura, C., Delande, D. & Müller, C. A. Coherent matter wave transport in speckle potentials. *New J. Phys.* **9,** 161 (2007).
28. Mahan, G. D. *Many Particle Physics* (Springer, 1990).
29. Lifshits, I. M., Gredeskui, S. A. & Pastur, L. A. *Introduction to the Theory of Disordered Systems* (Wiley, 1988).
30. Piraud, M., Sanchez-Palencia, L. & Van Tiggelen, B. Anderson localization of matter waves in 3D anisotropic disordered potentials. *Phys. Rev. A* **90,** 063639 (2014).
31. Fratini, E. & Pilati, S. Anderson localization of matter waves in quantum-chaos theory. Preprint at http://arXiv.org/abs/1503.04332 (2015).
32. McGehee, W. R., Kondov, S. S., Xu, W., Zirbel, J. J. & DeMarco, B. Three-dimensional Anderson localization in variable scale disorder. *Phys. Rev. Lett.* **111,** 145303 (2013).
33. Müller, C. A. & Shapiro, B. Comment on "Three-Dimensional Anderson Localization in Variable Scale Disorder". *Phys. Rev. Lett.* **113,** 099601 (2014).
34. McGehee, W. R., Kondov, S. S., Xu, W., Zirbel, J. J. & DeMarco, B. McGehee *et al.* Reply. *Phys. Rev. Lett.* **113,** 099602 (2014).
35. Huang, K. & Meng, H-F. Hard-sphere Bose gas in random external potentials. *Phys. Rev. Lett.* **69,** 644–647 (1992).
36. Nattermann, T. & Pokrovsky, V. L. Bose–Einstein condensates in strongly disordered traps. *Phys. Rev. Lett.* **100,** 060402 (2008).
37. Pilati, S., Giorgini, S. & Prokof'ev, N. Superfluid transition in a Bose gas with correlated disorder. *Phys. Rev. Lett.* **102,** 150402 (2009).
38. Crowell, P. A., Van Keulz, F. W. & Reppy, J. D. Onset of superfluidity in ^{4}He films adsorbed on disordered substrates. *Phys. Rev. B* **55,** 12620–12634 (1997).
39. Lye, J. E. *et al.* Bose–Einstein condensate in a random potential. *Phys. Rev. Lett.* **95,** 070401 (2005).
40. Zapf, V., Jaime, M. & Batista, C. D. Bose–Einstein condensation in quantum magnets. *Rev. Mod. Phys.* **86,** 563–614 (2014).

Acknowledgements

We acknowledge discussions with V. Josse and L. Pezzé. This work was supported by ERC (grants 247371 and 258325), and partially by EU - H2020 research and innovation programme (grant 641122), INFN (MICRA collaboration) and MIUR (grant RBFR08H058).

Author contributions

G.Semeghini and M.L. designed the experiment; G.Semeghini, M.L. and G.M. analysed the data and performed the numerical simulations; all the other authors participated to the experiment, data analysis, discussion of the results and writing of the manuscript.

Additional information

Supplementary information is available in the online version of the paper. Reprints and permissions information is available online at www.nature.com/reprints. Correspondence and requests for materials should be addressed to G.M.

Competing financial interests

The authors declare no competing financial interests.